# A Solid-State NMR Study of Phospholipid-Cholesterol Interactions: Sphingomyelin-Cholesterol Binary Systems

Wen Guo,* Volker Kurze,† Thomas Huber,‡ Nezam H. Afdhal,§ Klaus Beyer,¶ and James A. Hamilton‖
Departments of *Medicine and ‖Biophysics, Boston University School of Medicine, Boston, Massachusetts 02118 USA; †Department of Radiology, Technische Universität München, Munich, Germany; ‡Department of Chemistry, University of Arizona, Tucson, Arizona 85721, USA; §Beth Israel Hospital, Harvard Medical School, Boston, Massachusetts 02115, USA; and ¶Lehrstuhl für Stoffwechselbiochemie, Ludwig-Maximilians-Universität München, Munich, Germany

ABSTRACT We used solid-state NMR techniques to probe the interactions of cholesterol (Chol) with bovine brain sphingomyelin (SM) and for comparison of the interactions of Chol with dipalmitoylphosphatidylcholine (DPPC), which has a similar gel-to-liquid crystalline transition temperature. $^{1}$H-, $^{31}$P-, and $^{13}$C-MASNMR yielded high-resolution spectra from multilamellar dispersions of unlabeled brain SM and Chol for analysis of chemical shifts and linewidths. In addition, $^{2}$H-NMR spectra of oriented lipid membranes with specific deuterium labels gave information about membrane ordering and mobility. Chol disrupted the gel-phase of pure SM and increased acyl chain ordering in the liquid crystalline phase. As inferred from $^{13}$C chemical shifts, the boundaries between the ordered and disordered liquid crystalline phases ($L_{\alpha}^{o}$ and $L_{\alpha}^{d}$) were similar for SM and DPPC. The solubility limit of Chol in SM was ~50 mol %, the same value as previously reported for DPPC membranes. We found no evidence for specific H-bonding between Chol and the amide group of SM. The order parameters of a probe molecule, *d*31-*sn*1-DPPC, in SM were slightly higher than in DPPC for all carbons except the terminal groups at 30 mol % but were not significantly different at 5 and 60 mol % Chol. These studies show a general similarity with some subtle differences in the way Chol interacts with DPPC and SM. In the environment of a typical biomembrane, the higher proportion of saturated fatty acyl chains in SM compared to other phospholipids may be the most significant factor influencing interactions with Chol.

## INTRODUCTION

Sphingomyelin (SM) and phosphatidylcholine (PC) are major phospholipids in mammalian membranes. The proportions of these two phospholipids may modulate membrane structure, including the formation and stabilization of lipid rafts and caveolae (Simons and Ikonen, 2000). An increase in the SM/PC ratio has been recorded in atherosclerotic aorta lipids (Böttcher and van Gent, 1961) and in the lipid-rich particles isolated from advanced plaques (Chao et al., 1990); this increase may be a response to the higher levels of unesterified cholesterol (Chol) in mature plaques. It has been proposed that SM plays a role in stabilizing the bilayer membrane structure, especially in the presence of a high concentration of Chol (Cullis and Hope, 1980). In addition, increased Chol levels and SM/PC ratios in membranes, coupled with increased chain ordering in phospholipids, have been correlated with aging of cells and organs (Levi et al., 1989; Prisco et al., 1986; Lewin and Timiras, 1984; Aureli et al., 2000). Feeding Chol-enriched diets to rats resulted in an increased SM/PC ratio in the ileal brush border membrane (Keelan and Clandinin, 1997). In the human skin fibroblast, depletion of Chol activates the de novo synthesis of SM (Leppimäki et al., 1998), which potentiates recruitment of new Chol molecules into the membrane bilayers. This suggests that the SM/Chol ratio is under tight control by endogenous mechanisms.

Incorporation of Chol into SM bilayers decreases the acyl chain ordering in the gel phase and increases ordering in the liquid crystalline ($L_{\alpha}$) phase, analogous to its effects on PC. Pure SM membranes with asymmetric chains (i.e., chains with a pronounced difference in length) have partially interdigitated bilayers in the gel ($L_{\beta}$) phase, which is disrupted with incorporation of Chol (Lund Katz et al., 1988). Depending on the mixing ratio, phase separation may occur in the liquid crystalline phase of SM/Chol (Ahmed et al., 1997), similar to dipalmitoylphosphatidylcholine (DPPC)/Chol mixtures (Sankaram and Thompson, 1990).

Are there specific molecular features of SM that distinguish it from PC in its interactions with Chol? Several kinds of evidence suggest that Chol appears to interact more strongly with SM than PC. For example, compared to its effects on PC, Chol 1) condenses SM monolayers more tightly and desorbs from such monolayers more slowly (Ohvo and Slotte, 1996; Lund Katz et al., 1988; Needham and Nunn, 1990), 2) results in lower water permeability in SM bilayers (Lande et al., 1995), and 3) oxidizes more slowly in SM bilayers when exposed to oxidase (Slotte, 1992) and shows a transition in oxidation rate at the mixing ratio of $X_{\mathrm{Chol}} = 67$ mol % (Bittman et al., 1994). One hypothesis to explain these results is that Chol forms a strong H-bond to the amide-linkage in SM (Sankaram and Thompson, 1990). This hypothesis was supported by the observation that the oxidation of Chol by cholesterol oxidase was accelerated in SM/Chol monolayers or vesicles when the amide-linked acyl group was replaced with an

*Submitted October 1, 2001 and accepted for publication April 3, 2002*

Address reprint requests to James A. Hamilton, Boston University School of Medicine, 715 Albany St. W302, Boston, MA 02118-2394. Tel.: 617-638-5048; Fax: 617-638-4041; E-mail: hamilton@biophysics.bumc.bu.edu.



0006-3495/02/09/1465/14 $2.00

ester-linked acyl group, although Chol was equally miscible in both phospholipids (Bittman et al., 1994).

In contrast, other investigators have found no evidence of preferential interactions between Chol and either PC or SM in the liquid crystalline phase at any mixing ratio using x-ray diffraction (Calhoun and Shipley, 1979) or fluorescence techniques (Schroeder and Nemecz, 1989). Furthermore, no differences in the Chol exchange rate (Lange et al., 1979) or in the bilayer cohesive properties (McIntosh et al., 1992) were observed in SM/Chol compared to PC/Chol membranes when the acyl chain lengths were matched to give the same phase transition temperature without Chol.

In light of the recent debate on the existence of SM/Chol-rich rafts and their biological functions in the plasma membranes (Dobrowsky, 2000), new approaches are required to address the question of whether Chol interacts with SM more favorably than PC. In this work we investigated interactions of Chol with SM using $^{1}H$, $^{31}P$, $^{13}C$, and $^{2}H$ solid-state NMR methods. The findings were compared to PC/Chol interactions to identify effects of backbone and acyl chain modifications on phospholipid/Chol interactions.

## MATERIALS AND METHODS

### Materials

Bovine brain sphingomyelin (SM, >99% pure) was purchased from Avanti Polar Lipids (Alabaster, AL) and cholesterol (Chol, >99% pure) from Nuchek (Elysian, MN). Both lipids were used as received. The purity of selected samples was checked by TLC before and after NMR experiments. Sample degradation was not significant. According to the acyl chain analysis provided by the supplier, the brain SM contained 45.5% 18:0, 23.5% 24:0, 7.2% 22:0, 6.3% 24:1, 5.1% 20:0, 1.7% 16:0, and 10.9% other fatty acids with a total ratio of saturated to unsaturated fatty acids of $S/U = 13.1$. The very long chain fatty acids occur predominantly in the acyl chain. Deuterated cholesterol (3$\alpha$,3$\beta$-*ol*-cholesterol-*d*2) was prepared from cholest-5-en-3$\beta$-on essentially according to a published procedure (Wheeler and Mateos, 1958). The product purity was checked by TLC and $^{1}H$-NMR.

### Sample preparation

In all experiments the lipid compositions are expressed as $X_{Chol}$, the mol % of Chol with respect to total lipid. Hydrated bovine brain SM has a $L_\beta \rightarrow L_\alpha$ phase transition temperature ($T_m$) of ~39°C (McIntosh et al., 1992). Using standard DSC and MASNMR measurements, we confirmed similar phase transitions in fully hydrated (50 wt% $H_2O$) pure SM samples (data not shown). All the experiments presented in this work were performed either at 25°C (below $T_m$) or at 45°C (above $T_m$).

For MASNMR, lipid powders of SM and Chol were weighed in a 10-ml test tube, dissolved in chloroform, and mixed. The organic solvent was removed under dry nitrogen gas and the thin layer of lipids thus formed was further lyophilized overnight. Then, de-ionized water was added to hydrate the lipids with 50 wt % of water. The lipid mixture was further mixed by vigorous vortexing, followed by 5–10 freeze-thaw cycles to ensure homogeneity. The sample was then loaded into a 4 mm $ZrO_4$ rotor for MASNMR experiments.

For $^{2}H$-NMR, oriented samples were prepared according to the following procedure: 30 mg of the lipids was dissolved in 5 ml of deuterated methanol ($CH_3OD$). The solution was spread evenly on 50 ultrathin glass plates (8 × 18 × 0.08 mm; Marienfeld Lab. Glassware, Bad Mergentheim, Germany) and dried for 20 min under a flow of warm air and then at room temperature for at least 18 h in vacuo (20–30 Pa). The glass plates with the dried lipid deposits were stacked on top of each other with gentle pressure and inserted, along with a pair of glass cylinder segments, into an open glass tube of 9.8 mm i.d. as previously shown (Fig. 1 in Kurze et al., 2000). Two small paper strips were soaked in $D_2O$ and then dried carefully. $D_2O$ (4 $\mu$l) was spotted onto each of the dry strips and the strips were attached at the short side of the stack. The cylinder was rapidly stoppered by appropriately machined Teflon plugs with silicon o-rings, and the membranes were annealed for 4 h at 50°C. Further hydration was achieved by repeating the process once more until full hydration (~25–30 mol/mol) was achieved. The total time required for sample annealing was ~12 h. Stepwise hydration resulted in planar alignment of the membranes, whereas sudden addition of larger quantities of $D_2O$ sometimes led to the formation of vesicular structures as shown by $^{31}P$-NMR spectroscopy.

### NMR spectroscopy

$^{13}C$-, $^{1}H$-, and $^{31}P$-NMR experiments were performed on a Bruker (Billerica, MA) AMX300 NMR spectrometer equipped with solid-state NMR accessories as described before (Guo and Hamilton, 1995). A standard pulse sequence experiment was used for $^{1}H$, $^{13}C$, and $^{31}P$ nuclei, with a 90° pulse width of 12.0, 9.0, and 5.0 $\mu$s, respectively. Inverse-gated decoupling was used when observing $^{13}C$ and $^{31}P$ and the pulse sequence is designated "HPDEC." For selected experiments observing $^{13}C$, a CPMAS pulse sequence was used. The Hartman-Hahn condition was determined using glycine as the standard sample and was optimized using the manufacturer-provided standard protocol with 50 kHz power level for both the cross-polarization transfer and the decoupling periods. The same decoupling power was used to obtain $^{13}C$ spectra without CP. For $^{31}P$, 5 kHz decoupling power was sufficient to yield high-resolution spectra. The sample spinning rate was 4 kHz for $^{13}C$, and 1.7 kHz for $^{1}H$- and $^{31}P$-MASNMR experiments. Chemical shifts were referred to the external reference standards: glycine carbonyl carbon for $^{13}C$ (176.06 ppm), phosphoric acid for $^{31}P$ (0.0 ppm), and TMS for $^{1}H$ (0.0 ppm). Linewidths were measured using the Bruker deconvolution program assuming only Lorentzian contributions.

The $^{2}H$-NMR experiments were performed on a Varian VXR-400S spectrometer controlled by a Sun SparcStation5 running Solaris 2.5 and VNMR 5.1 software as described before (Kurze et al., 2000). The spectra were acquired using a 10-mm i.d. flat wire solenoid coil and a quadrupolar echo pulse sequence as provided by the manufacturer with composite pulses (pulse width: 7 $\mu$s, echo time: 20 $\mu$s, spectral width: 200 kHz, recycling time: 0.7 s). Zeroth- and first-order phase corrections and a multipoint spline fit for the baseline resulted in a spectral shape, as shown in Fig. 7 *B*. [Asymmetric peak heights and baseline irregularities are a consequence of such corrections. In view of our objective of obtaining sufficiently accurate peak positions, the used acquisition parameters were considered well suited for the purpose.] The rather long pulse width of 7 $\mu$s and the resulting inhomogeneous excitation of the spectrum have no influence on our interpretations, because we do not perform any peak integration.

To extract quadrupolar splittings from these spectra, Lorentzian lines were fitted according to the following procedure: for the inner splittings, only that part of the spectrum was used where only one resonance of one acyl chain segment dominated the shape of the spectrum. Influences of other resonances in this spectral region were accounted for by an underlying linear baseline fit. One Lorentzian at a time was fitted on top of an inclined baseline, using only a narrow region of the spectrum for the fitting procedure. In the area of overlapping signals, three Lorentzians and an inclined baseline were fitted simultaneously to simulate the envelope of resonances. Similar to the line-fitting procedure for the inner splittings, only that spectral region was fitted that was clearly distinct from other resonances. This procedure does not require a perfect symmetry of the acquired and phase-corrected spectra and still gives reliable and reproduc-

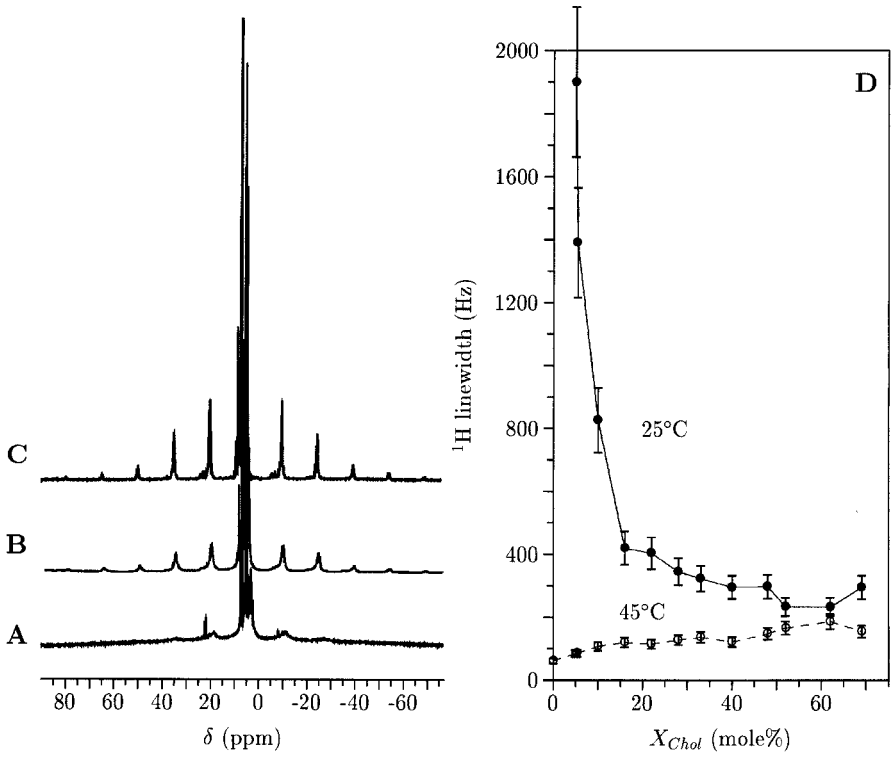


FIGURE 1 Bilayer $^1$H-MASNMR spectra of (*A*) SM at 25°C, (*B*) SM with 25% Chol at 25°C, and (*C*) SM at 45°C. (*D*) Linewidth of the first-order spinning sideband in $^1$H-MASNMR spectra of SM/Chol bilayers as a function of $X_{Chol}$. Error margins calculated from the respective signal-to-noise ratios.

ible values for quadrupolar splittings (Kurze, 1998; Kurze et al., 2000). A home-built goniometer was used for accurate sample orientation placing the glass plates at a right angle, and thus the bilayer normal parallel to the outer magnetic field. The central $D_2O$ signal arising probably from unoriented water was minimized with optimal annealing of the sample.

The magnitude of the quadrupolar splittings reflects combined effects of the interaction of the deuteron quadrupolar moment with the electric field gradient of their chemical bonds O–D and C–D [$\chi_{OD}$ = 220 kHz, $\chi_{CD}$ = 170 kHz (Mantsch et al., 1977)], the average orientation of the bilayer normal in the magnetic field [2nd Legendre polynomial $P_2(\cos\beta)$], with $\beta$ the angle between the bilayer normal and the external magnetic field and the orientational ordering of the membrane represented by the order parameter *S* (Davis, 1991; Marsan et al., 1999), according to Eq. 1:

$$\Delta\nu_Q = \tfrac{3}{2}\chi \cdot P_2(\cos\beta) \cdot S \qquad (1)$$

## RESULTS

### $^1$H-MASNMR spectra of the $L_\beta$ and $L_\alpha$ phase

$^1$H-MASNMR spectra were obtained above and below $T_m$ for fully hydrated SM membranes ($T_m$ = 39°C) with 0% to 70% Chol at 25°C and 45°C. Spectra of pure SM bilayers at 25°C and 45°C and bilayers with 25% Chol are shown in Fig. 1 (*left panel*). The center band for pure SM was detected as an envelope of signals (Fig. 1 *A*), because the SM used in this study contained a small proportion of unsaturated acyl chains, which remained in a mobile state at 25°C. The majority of the sample was in the $L_\beta$ phase, as evidenced by the very broad sideband signals. The sidebands originate predominantly from the resonance of the internal methylene $(CH_2)_n$ signal. The decrease in the sideband linewidths is indicative of the increased mobility associated with the elimination of the $L_\beta$ phase (Forbes et al., 1988) with increasing Chol (Fig. 1 *B*). At 45°C pure SM is in the $L_\alpha$ phase, and the $^1$H-MASNMR spectrum consists of sharp center bands flanked with sharp sidebands (Fig. 1 *C*).

The linewidth of the first-order sidebands of $^1$H-MASNMR spectra of SM is plotted as a function of $X_{Chol}$ in Fig. 1 *D*. At 25°C, the $^1$H linewidth of the $(CH_2)_n$ peak decreased rapidly with increasing $X_{Chol}$ up to ~15%, and displayed only a slight decrease with further addition of Chol (Fig. 1 *D*). This correlates with previous reports that the incorporation of Chol into SM gradually disrupts the bilayers in the $L_\beta$ phase (Lund Katz et al., 1988), and suggests that the $L_\beta$ phase in SM was eliminated when the $X_{Chol}$ was >15%.

The continuous slight increase in the $^1$H linewidth with increasing Chol at 45°C reflects the acyl chain ordering effect of Chol, which increases the spectral density at slow fluctuations and thereby the transverse relaxation rate. At all mixing ratios, spectra of SM membranes displayed broader $^1$H-MASNMR linewidths at 25°C than at 45°C.

### $^{31}$P-MASNMR

To investigate the effect of Chol on the phosphate headgroup, $^{31}$P-MASNMR spectra were obtained for SM with varying $X_{Chol}$ at 25°C and 45°C. Fig. 2 compares the $^{31}$P-

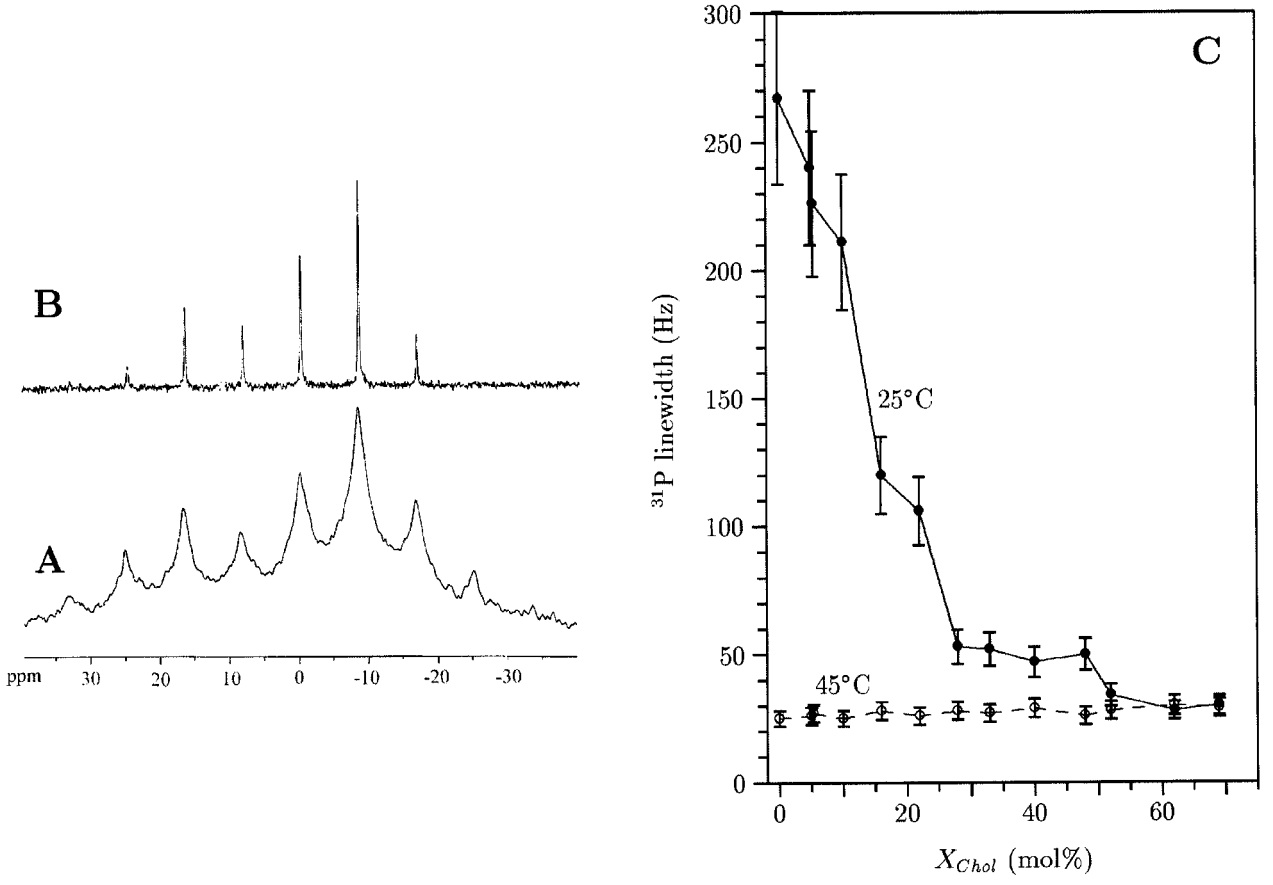


FIGURE 2 $^{31}$P-MASNMR spectra of (*A*) pure SM and (*B*) SM with 25% Chol at 25°C. (*C*) The linewidth of the first-order spinning sideband in the $^{31}$P-MASNMR specrum of SM/Chol bilayers as a function of $X_{Chol}$. Error margins calculated from the respective signal-to-noise ratios.

MASNMR spectra with $X_{Chol}$ of 0% (Fig. 2 *A*) and 25% (Fig. 2 *B*) at 25°C. The $^{31}$P spectra at 45°C were similar to those of Fig. 2 *B* (not shown). These spectra resemble typical $^{31}$P-MASNMR spectra of phospholipids as reported before (Griffin et al., 1978; Guo and Hamilton, 1995).

Fig. 2 *C* shows the $^{31}$P linewidth of the centerband obtained from MASNMR spectra of SM membranes at 25°C (●) and 45°C (○) as a function of $X_{Chol}$. At 25°C, the linewidth of the $^{31}$P center peak and the sidebands decreased rapidly with the addition of Chol up to ~25% (Fig. 2 *C*, ●) and then only slightly at higher $X_{Chol}$. These results agree with the concept that the insertion of Chol expands the cross-sectional headgroup area available to each lipid molecule, thereby increasing the headgroup mobility (Shepherd and Buldt, 1979). At 45°C the $^{31}$P linewidth showed little change with increased $X_{Chol}$ (Fig. 2*C*, ○).

We previously reported a line-broadening effect on the $^{31}$P resonance in MASNMR spectra with the addition of Chol beyond 50% in DPPC membranes, which was ascribed to the crystallization of Chol near the headgroup region (Guo and Hamilton, 1995). We did not observe such an effect in SM/Chol mixtures prepared by the identical protocol.

### $^{13}$C-MASNMR spectra of SM in the $L_\beta$ and $L_\alpha$ phases

$^{13}$C spectra provide numerous resolved resonances for investigating interactions of Chol with specific molecular segments in SM, especially the backbone region. $^{13}$C-MAS spectra can be obtained with and without cross-polarization (CP) to evaluate relative mobilities of different carbons in lipids (Guo and Hamilton, 1995, 1996). The high-resolution spectrum of SM in the $L_\alpha$ phase (45°C) obtained without CP to highlight carbons with relatively high mobilities (Fig. 3 *A*) is similar to MASNMR spectra of the other phospholipids in the $L_\alpha$ phase (Forbes et al., 1988). In a CPMAS experiment, signals from C=C, $NCH_3$, and a,b-$CH_2$ were reduced (Fig. 3 *B*), and the shorter CP contact time resulted in more complete attenuation (Fig. 3 *C*). At short CP-contact times, the signal intensity depends primarily on the effective strength of the dipole-dipole coupling between protons and $^{13}$C. Geometric factors and motions influence the strength of the dipole-dipole interaction. Under our conditions, the geometric factors for individual $CH_2$ or HC=CH groups remained the same with different contact times. Hence, the reduced CP enhancement (seen as signal

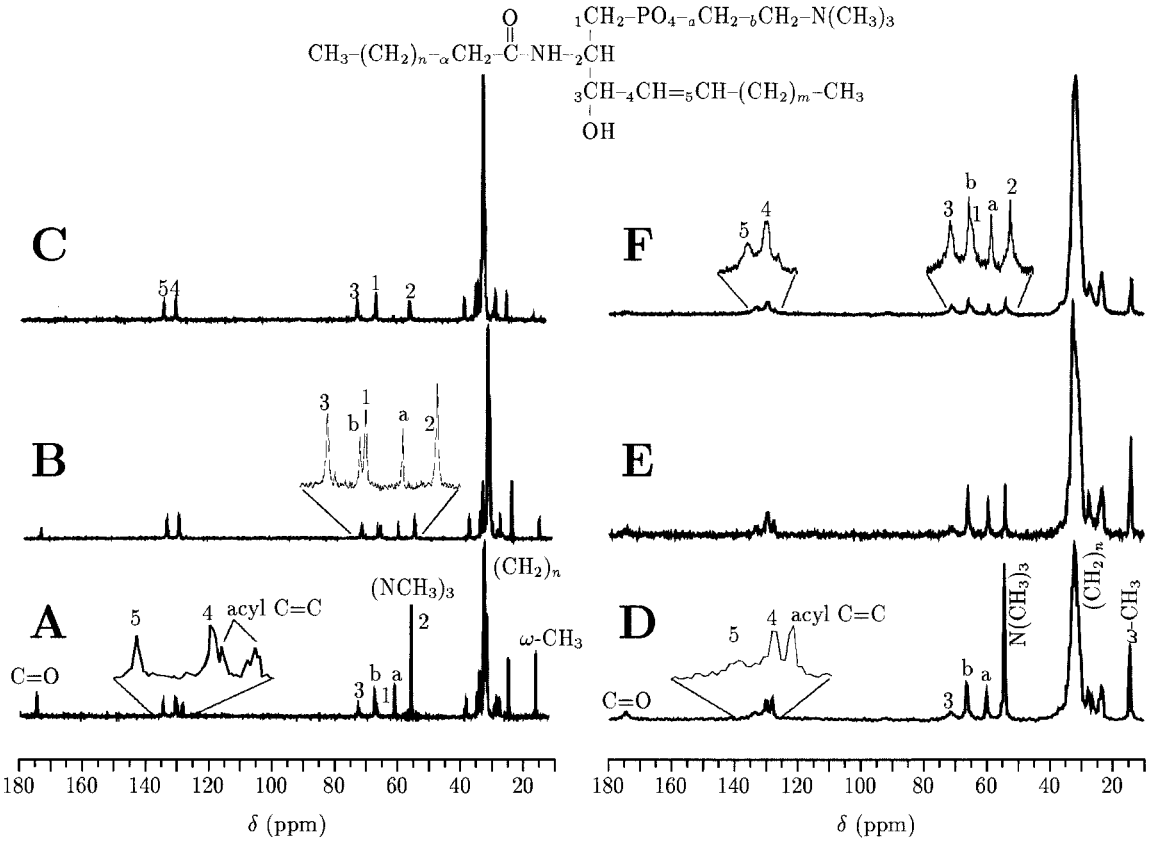


FIGURE 3 *Top:* Structural formula of SM with labels identifying the carbons assigned in the spectra. *Left panel:* $^{13}$C-MASNMR spectra of SM at 45°C without CP (*A*), with CP contact of 5 ms (*B*), and 1 ms (*C*). *Right panel:* $^{13}$C-MASNMR spectra of SM at 25°C without CP (*D*), with CP contact of 5 ms (*E*), and 1 ms (*F*).

attenuation when compared with the HPDEC spectrum) is likely a result of increased molecular motions or decreased orientational ordering. The observation that signals from the sphingosine backbone (SM(1) to SM(5)) have similar intensities in the spectrum with a short CP contact time (Fig. 3 *C*) indicates that these carbons have a similar mobility and are more rigid than other carbons in the molecule. [Although the C=O of the acyl chain is close to the glyceryl backbone and may have similar restricted motions, its intensity is not efficiently amplified by CP contact because of the lack of strong H-C dipolar interactions.]

In the $L_\beta$ phase at 25°C, the MASNMR spectrum of SM without CP (Fig. 3 *D*) showed narrow signals for the mobile carbons. Signals from the rigid carbons were broad, probably because of chemical shift inhomogeneity due to multiple microenvironments with slow chemical exchange. With CP, signals from the mobile carbons and the carbonyl were attenuated, whereas the broad signals for the rigid carbons were virtually unaffected, as expected (Fig. 3 *E* and *F*). In the $L_\alpha$ phase, the SM(4) and SM(5) peaks had similar linewidths (Fig. 3 *A*), but in the $L_\beta$ phase the SM(5) peak was much broader than SM(4) (Fig. 3 *D*). This reflects the low mobility of the paraffinic chains in the $L_\beta$ phase, probably as a result of interdigitation of acyl chains.

## The effects of Chol on $^{13}$C-MASNMR spectral features and the detection of crystalline Chol monohydrate

At low $X_{Chol}$ (<10%), the $^{13}$C-MASNMR spectral features were similar to those for pure SM (not shown). Beginning at 10%, Chol signals became apparent. Fig. 4 shows the spectral region of 110–150 ppm of SM with varying $X_{Chol}$ obtained with and without CP at 25°C and 45°C. The spectral regions of 10–110 ppm and 150–180 ppm (not shown) were generally similar to those for PC/Chol mixtures (Forbes et al., 1988; Guo and Hamilton, 1995). At 25°C without CP (Fig. 4 *A*), the peaks for SM(4) and SM(5) became narrower and better resolved as $X_{Chol}$ increased. These changes reflect the increasing disorder as a result of Chol incorporation into the $L_\beta$ phase. Alternatively, incorporation of Chol may cause phase changes into a more mobile state in local regions. These two possibilities cannot be distinguished with our data. At 45°C, the SM/Chol

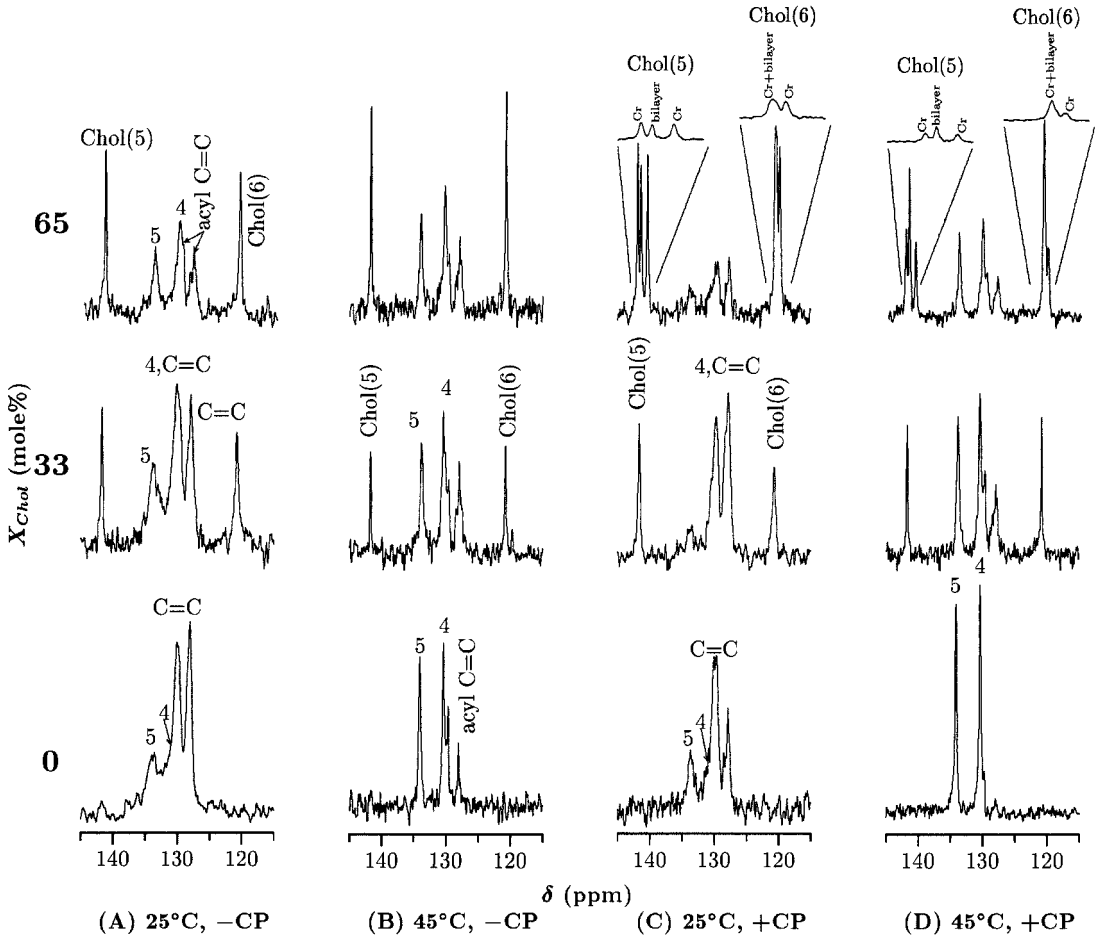


FIGURE 4 $^{13}$C-MASNMR spectra (110–190 ppm) of SM/Chol bilayers without CP at 25°C (*A*) and 45°C (*B*), and with CP (contact time: 5 ms) at 25°C (*C*) and 45°C (*D*) at various Chol concentrations. The SM(4) resonance overlaps with the doublet representing the acyl C=C. "Cr": signals from crystalline cholesterol monohydrate.

mixtures were in the $L_\alpha$ phase regardless of $X_{\mathrm{Chol}}$ (0–70%), and there were no significant effects of $X_{\mathrm{Chol}}$ on the spectral features of SM (Fig. 4 *B*) except for the relative peak intensities reflecting changes in the sample composition.

The effects of Chol on SM as observed in CPMAS spectra were more complicated. At 25°C, with $X_{\mathrm{Chol}} = 0\%$ (Fig. 4 *C*) and 10% (not shown), both the acyl C=C and the SM(4) and SM(5) resonances were detected. The incorporation of Chol reduced the signal intensities from the SM(4) and SM(5) carbons relative to the acyl C=C signal. However, at 45°C the opposite result was observed (Fig. 4 *D*): the SM(4) and SM(5) signals became relatively more intense than the acyl C=C signal with $X_{\mathrm{Chol}}$ of 0–10%. The diminished acyl C=C signal was due to the higher mobility of these segments at this temperature, which would lead to a signal attenuation with CP. With the addition of Chol, the signals from acyl C=C became enhanced (Fig. 4 D, *middle*, *top*), reflecting decreased acyl chain mobility. We do not attribute such changes to geometric factors, because at 45°C the acyl chains containing the double bonds are essentially in a liquid-like state.

When the Chol content exceeds the saturation limit in phospholipid membranes, crystalline Chol monohydrate (CholM) forms (Guo and Hamilton, 1995). In general, for choline phospholipids the saturation limit is ~50% Chol (Bourgès et al., 1967), although a higher solubility (65%) has been reported (Huang et al., 1999). Because differences in sample preparation may affect this determination, we used identical procedures for preparation of SM/Chol samples as for DPPC/Chol samples in our previous study (Guo and Hamilton, 1995). In SM/Chol mixtures we detected CholM when $X_{\mathrm{Chol}}$ was above 60%, as in the case of DPPC/Chol mixtures (Guo and Hamilton, 1995). Because of the low sensitivity of natural abundance $^{13}$C-NMR, we were not able to determine more precisely the mixing ratio of Chol at which crystallization began.

The $^{13}$C-MASNMR spectrum of SM/Chol with $X_{\mathrm{Chol}}$ of 65% obtained at 45°C with CP (Fig. 4 *D*, *top*) shows three

resonances for the Chol(5) signal, the outer two resonances representing CholM (Guo and Hamilton, 1995, 1996), and the center signal for Chol in the liquid crystalline phase. The downfield peak of the Chol(6) twin peaks in CholM overlaps with the signal from the Chol(6) in bilayer phases, as in the case of the DPPC/Chol mixtures (Guo and Hamilton, 1995).

### Effects of Chol on the chemical shifts of C=O group in SM

Effects of Chol on the carbonyl region of SM were reflected in the chemical shifts of the C=O group ($\delta_{CO}$). Although chemical shift should be independent of the experimental protocol, in a simple system with coexisting phases of different mobility ($L_\alpha$ vs. $L_\beta$), CPMAS and HPDEC each selectively enhance resonance signals of lipids of the $L_\beta$ and $L_\alpha$ phases, respectively. [As both CPMAS and HPDEC spectra were acquired with the same decoupling conditions, the differences in the C=O resonance are not likely a result of sample temperature changes caused by RF heating.] Because the signal intensity of C=O was attenuated by CP at 25°C, only the $^{13}$C chemical shifts measured without CP contact were analyzed, and the results reflect the changes in the $L_\alpha$ phase. At 25°C, $\delta_{CO}$ increased gradually with increasing $X_{Chol}$ up to ~50% Chol, where it leveled off (Fig. 5 *A*). [A small mobile fraction exists in pure SM at 25°C as a result of phase separation due to chain unsaturation. Addition of Chol increases the pool size of this mobile phase, as evidenced by the changes in the $^1$H and $^{31}$P linewidths (Figs. 1 and 2). However, incorporation of Chol increases the acyl chain ordering and increases the $^{13}$C chemical shifts (Guo and Hamilton, 1995).] At 45°C, $\delta_{CO}$ was not significantly affected by $X_{Chol}$ up to ~25%, but then increased with increasing $X_{Chol}$ until leveling off at $X_{Chol} > 50\%$.

### Effects of $X_{Chol}$ on the chemical shifts of internal methylene $(CH_2)_n$ in SM

The chemical shift $\delta_{CH_2}$ of the composite resonance of internal methylenes [$(CH_2)_n$] reflects the ratio of *trans/gauche* conformations in the hydrocarbon chains (VanderHart, 1981). A novel feature of the $^{13}$C-MAS experiment is that the mobile and immobile $CH_2$ groups can be detected selectively. At 25°C the HPDEC experiment detected the hydrocarbon chains of pure SM membranes in the $L_\alpha$ phase at 31.7 ppm (Fig. 5 *B*, *), whereas CPMAS detected the hydrocarbon chains in the $L_\beta$ phase at 32.8 ppm (Fig. 5 *B*, ●). In both experiments the decoupler power and the acquisition time were the same. It is unlikely that the RF heating in the HPDEC experiment results in the observed chemical shift. The downfield shift is more likely to reflect a lower fraction of *gauche* conformations in the $L_\beta$ phase. The addition of Chol increased the ordering of the $L_\alpha$ phase, as reflected in the increased $\delta_{CH_2}$, while reducing the ordering in the $L_\beta$ phase (decrease in $\delta_{CH_2}$ for $0 \leq X_{Chol} \leq 15\%$). At $X_{Chol} \approx 15\%$, which corresponds to the $L_\beta \rightarrow L_\alpha$ phase transition detected with the $^1$H linewidth (Fig. 1), the two resonances converged to the same value.

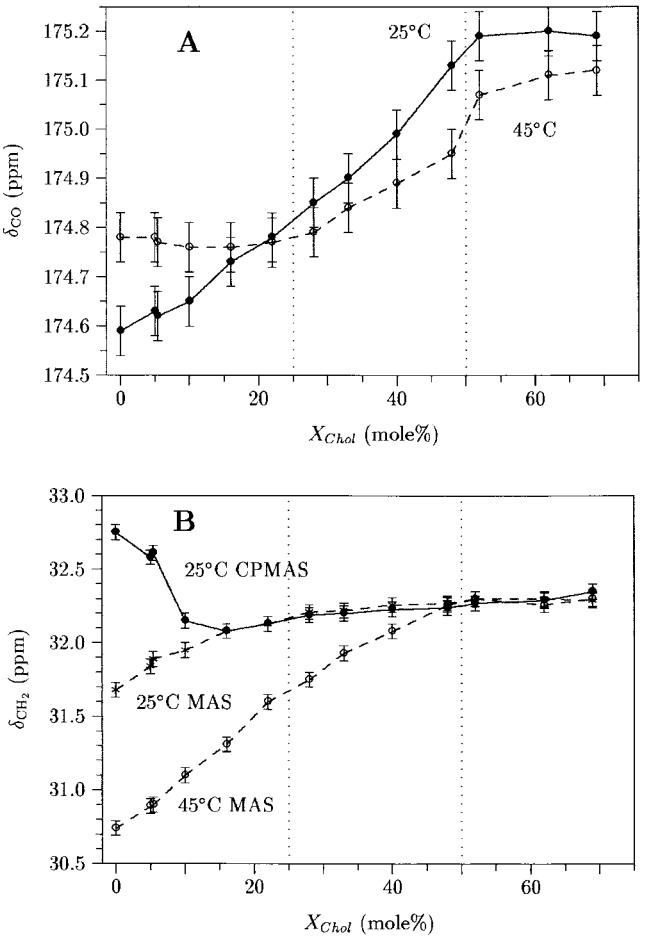


FIGURE 5 The $^{13}$C chemical shift of the carbonyl group ($\delta_{CO}$, *A*) and the internal methylenes ($\delta_{CH_2}$, *B*) in SM as a function of Chol content. Error margins calculated from linewidths and signal-to-noise ratios.

At 45°C, the methylenes of pure SM in the $L_\alpha$ phase exhibited a chemical shift of $\delta_{CH_2} = 30.7$ ppm (Fig. 5 *B*, ○), the same as that of DPPC in the $L_\alpha$ phase (Guo and Hamilton, 1995). Addition of Chol resulted in a continuous increase of $\delta_{CH_2}$ (Fig. 5 *B*) with a slight decrease in the slope (for analysis cf. Discussion) at ~25% Chol, though not as significant as that observed in DPPC/Chol mixtures (Guo and Hamilton, 1995). The net change in $\delta_{CH_2}$ from pure SM to SM/Chol mixtures with $X_{Chol} = 50\%$ in the $L_\alpha$ phase was $1.5 \pm 0.1$ ppm, slightly higher than that found in DPPC/Chol mixtures ($1.3 \pm 0.1$ ppm).

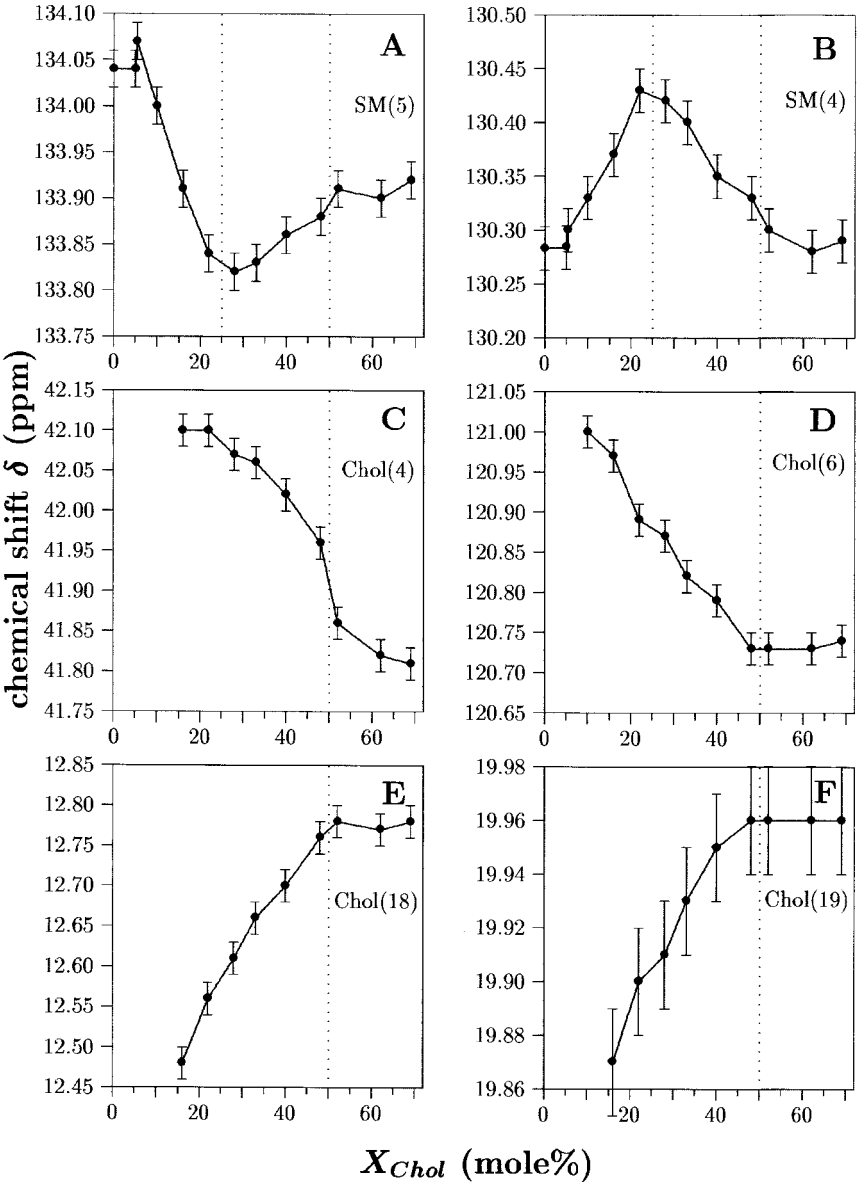


FIGURE 6 $^{13}C$ chemical shift $\delta$ of the selected carbon resonances of SM and Chol in the SM/Chol bilayers at 45°C as a function of Chol content $X_{Chol}$. Error margins calculated from linewidths and signal-to-noise ratios.

### Effects of $X_{Chol}$ on the chemical shifts of other carbons in SM and Chol

The chemical shifts of selected carbon resonances in $^{13}C$-MASNMR spectra of Chol and SM at 45°C are shown in Fig. 6 as a function of $X_{Chol}$; $\delta_{SM(5)}$ (Fig. 6 *A*) decreased with increasing $X_{Chol}$ to a minimum value at ~25%, above which it increased with increasing $X_{Chol}$. In contrast, $\delta_{SM(4)}$ (Fig. 6 *B*) increased with increasing $X_{Chol}$ to a maximum value at ~25%, then decreased with further Chol incorporation. Both $\delta_{SM(4)}$ and $\delta_{SM(5)}$ leveled off above 50%, where crystallization of Chol monohydrate occurs.

The transition point around $X_{Chol} \approx 25\%$ corresponds to that detected by $\delta_{CO}$ and $\delta_{CH_2}$ of SM (Fig. 5). The opposite trends of $\delta_{SM(4)}$ and $\delta_{SM(5)}$ may reflect an induced shift of electron cloud density along the double bond induced by the SM paraffinic chain interaction with Chol. The dependencies of $^{13}C$ chemical shifts on $X_{Chol}$ provide evidence for phase boundaries at 25 and 50% Chol, and suggest the coexistence of ordered and disordered liquid crystalline phases ($L_\alpha^o$; $L_\alpha^d$) between 25 and 50% Chol (cf. Discussion).

Fig. 6 *C–F* show the chemical shift of resonances of selected Chol carbons [Chol(4), Chol(6), Chol(18), and Chol(19)] at 45°C. The changes in $\delta_{Chol(21)}$ (not shown) were similar to those of $\delta_{Chol(19)}$. Signals from other Chol carbons either overlapped with the SM signals or showed only insignificant changes (not shown). Irrespective of whether the signals shifted upfield ($\delta_{Chol(4)}$ and $\delta_{Chol(6)}$) or downfield ($\delta_{Chol(18)}$ and $\delta_{Chol(19)}$), the chemical shifts of these Chol carbons all leveled off at ~50% Chol. For these resonances there were no marked transition points at lower Chol; however, the inability to detect

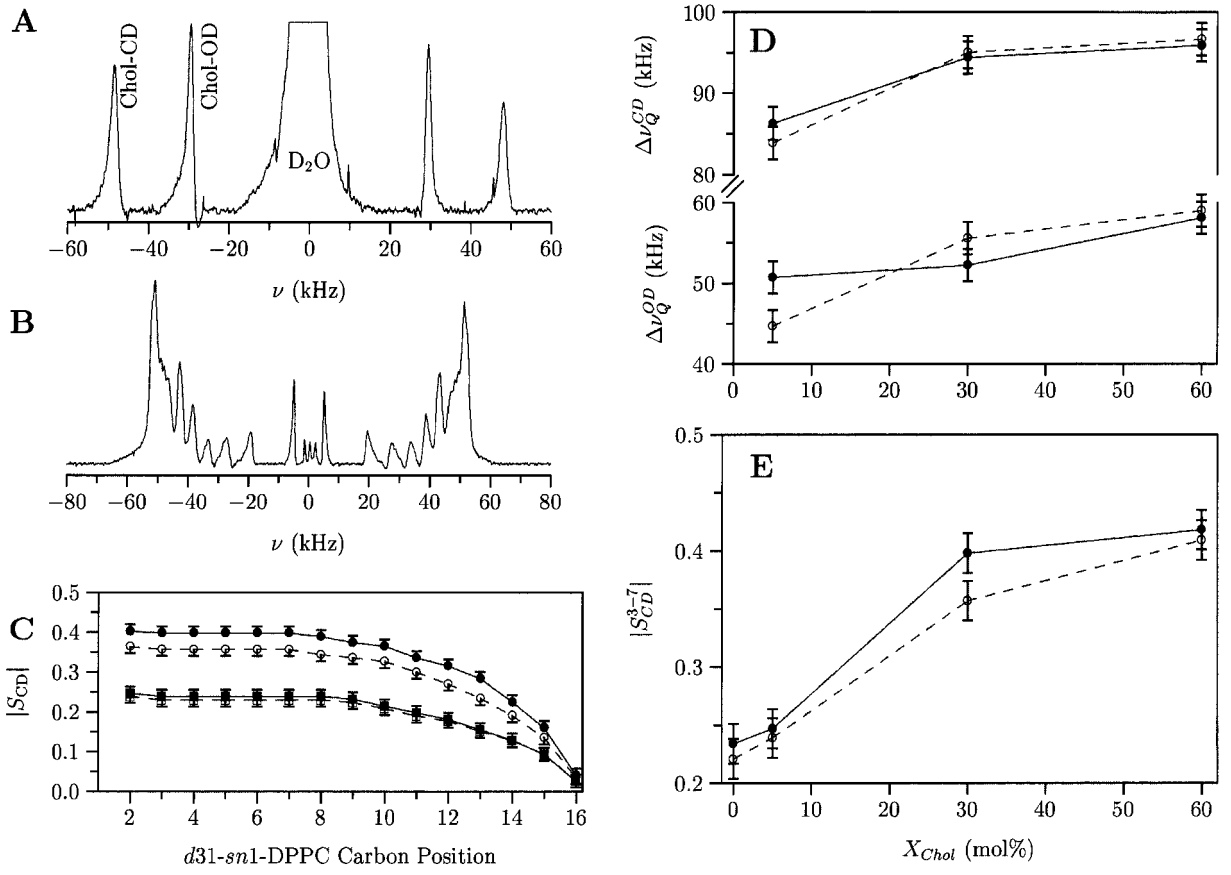


FIGURE 7 (*A*) $^2$H-NMR spectrum of Chol-*d*2 (60%) in $D_2O$-hydrated oriented DPPC membranes at 47°C. (*B*) $^2$H-NMR spectrum of *d*31-*sn*1-DPPC bilayers with 60% Chol at 47°C. (*C*) Order parameters of *d*31-*sn*1-DPPC in SM (45°C) and DPPC (47°C), with 30% Chol (SM: ●, DPPC; ○) and 5% Chol (SM: ■, DPPC: □). (*D*) Quadrupolar splittings of the CHol-CD ($\Delta\nu_Q^{CD}$) and Chol-OD ($\Delta\nu_Q^{OD}$) and as a function of $X_{Chol}$ in SM (45°C, ●) and DPPC (47°C, ○) membranes. (*E*) Order parameter of the carbon segments 3 to 7 ($S_{CD}^{3-7}$ of *d*31-*sn*1-DPPC (5%) in SM (45°C, ●) and DPPC (47°C, ○) membranes as a function of $X_{Chol}$. Error margins calculated from linewidths and signal-to-noise ratios.

Chol signals at $X_{Chol} < 15\%$ compromises the analysis of the data in this region.

## Orientational ordering of Chol and phospholipid acyl chains in SM and DPPC bilayers in the $L_\alpha$ phase by $^2$H-NMR

$^2$H-NMR spectra of labeled Chol-*d*2 were obtained from macroscopically oriented membranes of SM or DPPC with varying concentrations of Chol hydrated with $D_2O$. The samples were oriented such that the bilayer normal pointed in the direction of the external magnetic field. The experiments on DPPC were performed to allow comparisons with SM and complement earlier MASNMR experiments on DPPC/Chol mixtures (Guo and Hamilton, 1995). The main phase transition temperature of DPPC ($T_m$ = 41.1°C, Shipley et al., 1974) is very close to that of brain SM ($T_m \sim$ 39°C, McIntosh et al., 1992). Thus, DPPC can be considered a glycero-phospholipid analog to brain SM when comparing interactions with Chol.

Spectra were obtained at 45°C (SM) and 47°C (DPPC), equivalent reduced temperatures above their $T_m$. $X_{Chol}$ = 60% was used to assure that the $L_\alpha$ phase is saturated by Chol (cf. Discussion).

Fig. 7 illustrates spectra of DPPC with labeled Chol (7 *A*) and with labeled DPPC (7 *B*). Both spectra showed a narrow splitting (~2 kHz) for membrane-associated water, which has a residual orientational ordering arising from its interactions with the lipid membranes (not shown in 7 *A*). The central signal represents water that is not interacting with lipid membranes and therefore shows no preferred orientation and no quadrupolar splitting (small resonance at 0 kHz shown in Fig. 7 *B*). The appearance of a signal for isotropic water indicates full hydration of the membranes with a surplus of water (Kurze, 1998). The HDO signals are much less intense in Fig. 7 *B* because deuterium-depleted water was used to permit observation of DPPC signals close to the water peak.

In the spectrum of DPPC with $X_{Chol}$ = 60% (Fig. 7 *A*), the signals arising from the Chol deuterons are far apart from the central water signal, and much less intense. The

inner quadrupolar doublet ($\Delta\nu_Q^{OD} \approx 58$ kHz) represents the exchangeable $\beta$-hydroxyl deuteron of Chol (Chol-OD), the outer doublet ($\Delta\nu_Q^{CD} \approx 96$ kHz), the $\alpha$ deuteron covalently bound to the Chol(3) carbon (Kurze, 1998; Kurze et al., 2000). The $^2$H-NMR spectral features of Chol-*d*2 in oriented $D_2O$-hydrated SM (not shown) were similar to those for the DPPC bilayers and those of Chol-*d*2 in palmitoyl-oleyl-PC bilayers (Kurze et al., 2000).

To compare the hydrocarbon chain ordering in SM/Chol and DPPC/Chol binary mixtures, we used deuterium-labeled DPPC (*d*31-*sn*1-DPPC) as a probe molecule (5%) in DPPC or SM membranes with unlabeled Chol hydrated with deuterium-depleted water. As shown in Fig. 7 *B* (DPPC membranes with $X_{Chol} = 60\%$ at 47°C), the spectra displayed an envelope of quadrupolar doublets symmetrical around a small central signal representing residual deuterium in water (cf. above). After fitting Lorentzian lineshapes to this spectrum (see Methods), the splittings $\Delta\nu_Q$ of the quadrupolar doublets were extracted.

*d*31-Palmitoyl chain order parameter profiles ($|S_{CD}|$ as a function of methylene segmental position) both in a DPPC/Chol and SM/Chol bilayer were obtained using Eq. 1. The splittings were assigned to carbon chain positions according to magnitude. This assignment is most probably correct for the narrower splittings, whereas the assignment was uncertain in the plateau region where splittings overlap. Assigning the broadest splitting to the methylene in position 2 is arbitrary, and we did not assign the broader splittings to exact methylene positions rigorously. Fig. 7 *C* shows the order parameter profiles in SM and DPPC membranes with $X_{Chol} = 5\%$ and 30%. Although the profiles are not significantly different for 5% Chol (and 60% Chol, not shown), for 30% Chol the order parameters in the SM matrix were consistently slightly higher compared to the DPPC matrix, except for carbons 14–16. Near the center of the bilayer the acyl chains experience considerable motional freedom, resulting in smaller order parameters for the terminal segments of the acyl chain and smaller distinctions among our samples (Oldfield et al., 1978).

The quadrupolar splittings $\Delta\nu_Q^{CD}$ and $\Delta\nu_Q^{OD}$ obtained for Chol-CD and Chol-OD (Fig. 7 *A*) in SM and DPPC membranes are plotted in Fig. 7 *D* at three Chol concentrations. With increasing $X_{Chol}$ the splittings increase. Because the Chol molecules undergo rapid rotation around their principal axis (Seelig and Seelig, 1977; Dufourc et al., 1984) and rapid lateral diffusion within the membrane (Seelig and Seelig, 1977), the increase in quadrupolar splittings can be explained only by an increased ordering of the membranes. This increased ordering can be associated with a decrease of chain fluctuations, which results in a decrease of the most probable tilt angle of the the molecular axis of the Chol molecules. Oldfield et al. reported a method of calculating this most probable tilt angle from molecular order parameters assuming a Gaussian distribution of tilt angles (Oldfield et al., 1978). From the measured quadrupolar splittings we obtained order parameters $S_\alpha = \frac{2}{3}\Delta\nu_Q^{CD}/170$ kHz and calculated the tilt angles for all $X_{Chol}$ (Table 1).

**TABLE 1 Tilt angle of Chol in SM and DPPC membranes at three Chol concentrations; SM membranes at 45°C, DPPC membranes at 47°C**

| $X_{Chol}$ [%] | 5 | 30 | 60 |
|---|---|---|---|
| SM | 20.9° | 18.3° | 17.8° |
| DPPC | 21.7° | 18.1° | 17.6° |

Within error margins $\Delta\nu_Q^{CD}$ shows no significant difference of the orientational ordering of the Chol(3$\alpha$) C-D bond for SM (●) and DPPC (○) membranes, yet $\Delta\nu_Q^{OD}$ differs in SM and DPPC membranes at 5 and 30% Chol. At 60% Chol, $\Delta\nu_Q^{OD}$ is identical in both phospholipid membranes. Within error margins (±0.8°) the angles decrease significantly with increasing $X_{Chol}$, indicating a decrease in membrane mobility and undulations. At the same Chol concentration, though, the tilt angles do not differ significantly in SM and DPPC membranes.

The most intense splitting observed in spectra of *d*31-*sn*1-DPPC (Fig. 7 *B*) represents several methylene deuterons leading to the plateau region of the order parameter profiles (Fig. 7 *C*, carbon segments 3 to 7). Fig. 7 *E* shows the order parameter of the plateau region $|S_{CD}^{3-7}|$ for SM (●) and DPPC (○) membranes as a function of Chol content. At $X_{Chol}$=0, 5, and 60% $|S_{CD}^{3-7}|$ is not significantly different in SM and DPPC membranes, but at 30% Chol, $|S_{CD}^{3-7}|$ is somewhat higher for SM than for DPPC membranes.

## DISCUSSION

To elucidate molecular interactions and phase behavior in SM bilayers with Chol, we used $^1$H- and $^{31}$P-MASNMR experiments to evaluate molecular motions in the hydrocarbon interior and the polar interface, respectively. $^{13}$C-MASNMR experiments monitored molecular motions and local molecular environments throughout the SM structure and in parts of the Chol molecule. $^2$H solid-state experiments quantified molecular ordering and orientation of Chol and ordering of SM. These NMR approaches are advantageous in that they directly measure abundant NMR signals from various molecular segments in Chol and phospholipids ($^{13}$C, $^1$H, $^{31}$P) or signals from specifically enriched sites ($^2$H) without introducing perturbing molecular probes or chemical reactions. New insights into the phase behavior of SM with Chol and local interactions characteristic of the various phases are discussed below.

### Phase separation below and above $T_m$

As with other Chol-phospholipid binary mixtures, incorporation of Chol into SM *below* $T_m$ gradually diminished the amount of the gel phase and increased the liquid crystalline pool. This process was detected by monitoring simulta-

neously the changes in the two phases by $^{13}$C-MASNMR with (gel) and without (liquid crystalline) CP. At 25°C the gel phase was completely abolished at $X_{Chol} \sim 15\%$, as determined by $^{13}$C (Fig. 5 *B*) and $^{1}$H data (Fig. 1). The linear change in $\delta_{CO}$ with $X_{Chol}$ in the range of 15–50% suggests no phase separation in the liquid crystalline phase at 25°C.

Phase separation *above* $T_m$ has been documented for PC/Chol mixtures of varying acyl chain lengths (Vist and Davis, 1990; Huang et al., 1993; Sankaram and Thompson, 1991). Less information is available for SM/Chol (Sankaram and Thompson, 1990). In our study, the marked changes in chemical shifts of SM carbons in the interfacial region provide evidence for phase separation above 45°C. Phase separation boundaries are suggested by the $^{13}$C chemical shifts of CO, SM(4), and SM(5), which showed discontinuities at $X_{Chol} \sim 22\%$ and $\sim$50% (Figs. 5 and 6), implying the appearance of subphases at these ratios. Because all chemical shift values plateau at $X_{Chol} \sim$50%, the liquid crystalline phase at this ratio was likely saturated with Chol and reached the maximum orientational ordering inducible by Chol, characteristic of the $L_\alpha^o$ subphase.

Theoretically, a phase discontinuity at $X_{Chol} \sim 20\%$ is predictable, as this is the ratio at which free phospholipid domains disappear (Hui, 1993). Our observation of the changes in the chemical shifts at $\sim$22% is in close agreement with this prediction. Hence, analogous to our previous findings with DPPC/Chol mixtures (Guo and Hamilton, 1995), the phase diagram of SM/Chol bilayers at 45°C can also be divided into three ranges according to $X_{Chol}$. In range I, a disordered liquid crystalline phase ($L_\alpha^d$); in range II, an ordered liquid crystalline phase ($L_\alpha^o$) appears and coexists with $L_\alpha^d$; in range III, $L_\alpha^o$ and crystalline Chol coexist. The molecular exchange among these subphases (except for crystalline Chol) was fast on the NMR time scale (fast chemical exchange), as only one set of narrow NMR resonance was detected at any single $X_{Chol}$. The detected chemical shifts in range I or II reflect the population averages of the coexisting subphases and vary with the changes in pool sizes of the coexisting subphases.

The phase boundaries between range I and II detected by NMR are higher than those derived from ESR studies of brain SM/Chol (Sankaram and Thompson, 1990), and predict a wider range in which $L_\alpha^d$ and $L_\alpha^o$ subphases coexist. The ESR data (hyperfine splitting constants) show little or no dependence on Chol content in the range of 22–50%, where our chemical shift data show large changes. This discrepancy may be a result of the insensitivity of ESR to changes detected by NMR.

## Interactions between SM and Chol in the polar region in comparison with those in DPPC/Chol bilayers

As noted above, phase separation above $T_m$ detected by $^{13}$C-MASNMR in SM/Chol bilayers was similar to that found in DPPC/Chol bilayers. If the paraffin chain and the acyl chain in SM are considered structural analogs for the *sn*1 and *sn*2 acyl chains in DPPC, then the similarity in chemical shift changes in the polar region between these two systems is rather striking. At 45°C, both $\delta_{CO}$ in SM and $\delta_{CO(sn2)}$ in DPPC remained nearly unchanged until $X_{Chol}$ reached $\sim$22–25%, and then increased with increasing $X_{Chol}$. The $\delta_{SM(5)}$ of the paraffin chain in SM varied with the same pattern as that of $\delta_{CO(sn1)}$ in DPPC: both shifted upfield with increasing $X_{Chol}$ up to 25% and then shifted downfield with higher $X_{Chol}$. The changes in $\delta_{SM(5)}$ were paralleled by an opposite change in $\delta_{SM(4)}$ probably because of the induction effects of the double bond between SM(4) and SM(5). Taken together, the data suggest that conformational changes induced by Chol in the polar region of the glycerol or sphingosine backbones are similar. Chemical shifts of both SM carbonyl and DPPC *sn*2 carbonyl were insensitive to low $X_{Chol}$ but became significantly dependent on $X_{Chol}$ after the $L_\alpha^o$ subphase appeared. A possible interpretation is that in the $L_\alpha^d$ phase, SM molecules adopted an average orientation that led to stronger perturbations or interactions between the paraffinic chain and Chol. This arrangement changed in the $L_\alpha^o$ phase when the interactions between the interior acyl chain and Chol became stronger, and/or the probability of Chol interacting with both chains increased with increasing $X_{Chol}$, leading to rapid changes in the corresponding $\delta_{CO}$ values. If this model is applicable below $T_m$, it also explains the linear increase of $\delta_{CO}$ with $X_{Chol}$ (0–50%) at 25°C (Fig. 5 *A*). At this temperature the liquid crystalline pool was small and Chol preferentially incorporated in this small pool, influencing $\delta_{CO}$ even when the overall $X_{Chol}$ was low.

Another probe of the interfacial region suggested similarities between DPPC and SM in their interactions with Chol. The quadrupolar splitting ($\Delta\nu_Q^{CD}$) of the Chol(3$\alpha$)-CD was the same in both SM and DPPC bilayers at intermediate (30%) and high (60%) $X_{Chol}$ above $T_m$ (Fig. 7 *D*). This indicates similar molecular ordering and orientation of the Chol molecules in the two different host lipid bilayers. Furthermore, although the tilt angle was affected by Chol content (Table 1), it was the same for SM and DPPC at a given $X_{Chol}$.

## Interactions of Chol with SM and DPPC in the nonpolar region

The most significant differences between SM and DPPC are seen in the interactions within the hydrophobic area, the main segments involved in the van der Waals interactions with Chol. This was evaluated by the changes in the $^{13}$C chemical shifts and the order parameters of the internal methylenes (C4-C14).

As shown in Fig. 5 *B*, $\delta_{CH_2}$ in SM shifts downfield with $X_{Chol}$ in a linear manner, as reported for DPPC (Guo and Hamilton, 1995), with a change in the corresponding slopes

when the $L_\alpha^o$ subphase appears. However, this phase separation was correlated with a large change in slope from $(4.3 \pm 0.4) \cdot 10^{-2}$ to $(0.9 \pm 0.5) \cdot 10^{-2}$ ppm/mol % in DPPC (Guo and Hamilton, 1995), in contrast to a moderate change from $(3.9 \pm 0.5) \cdot 10^{-2}$ to $(2.6 \pm 0.5) \cdot 10^{-2}$ ppm/mol % in SM (Fig. 5 *B*). Because $\delta_{CH_2}$ reflects the ratio of *gauche/trans* conformations in the hydrocarbon chains, the increase in $\delta_{CH_2}$ with $X_{Chol}$ reflects the chain ordering effect of Chol. At lower $X_{Chol}$ *gauche* conformations dominated in both SM and DPPC, and the progressive incorporation of Chol led to an increased *trans/gauche* ratio. Therefore, the slopes are similar in both systems in this region. The somewhat lower slope in SM-Chol probably reflects the higher ordering of SM bilayers compared to DPPC bilayers in the absence of Chol (Fig. 7 *C*, see below). When domains of free DPPC disappeared and the $L_\alpha^o$ subphase appeared, the chain-ordering effect of Chol in DPPC bilayers was nearly maximal, so that further increases in $X_{Chol}$ only led to minor increases in $\delta_{CH_2}$. In SM, however, Chol-induced chain ordering continued to increase significantly after the appearance of an $L_\alpha$ subphase. This discrepancy is due at least in part to the fact that DPPC has two saturated hydrocarbon chains with 16 carbons, whereas the bovine SM contained a small fraction of unsaturated chains and each molecule had one chain of 16-18 carbons and the other of 20-24 carbons. Therefore, even after the disappearance of free SM clusters and the appearance of the $L_\alpha^o$ subphase, the incorporation of Chol continues to increase the chain ordering until $X_{Chol} \sim 50\%$. Whether this also indicates an overall "stronger" interaction of Chol with SM than with DPPC cannot be unambiguously determined by these results. However, it is clear that Chol-induced acyl chain ordering is more significant at intermediate mixing ratios in SM than in DPPC.

To address this issue further, we used $^2$H-NMR to probe the orientational ordering of the bilayers. Because of the difficulty in obtaining $^2$H-labeled SM, our strategy was to incorporate a small fraction of $^2$H-labeled DPPC (*d*31-*sn*1-DPPC, 5 mol %) into the SM/Chol bilayer. Parallel experiments were performed with DPPC/Chol. The order parameters obtained from SM membranes were consistently slightly higher than those from DPPC membranes (Fig. 7). Particularly noteworthy was the more significant increase in ordering with 30% Chol.

The order parameters ($S_{CD}^{3-7}$) of carbons 3-7 of *d*31-*sn*1-DPPC in both DPPC and SM bilayers increased with $X_{Chol}$, consistent with the chain ordering effect of Chol in lipid bilayers (Fig. 7 *E*). The slightly higher $S_{CD}^{3-7}$ at 0% Chol is consistent with the findings reported by Neuringer et al. (1979). However, the difference in $S_{CD}^{3-7}$ between SM and DPPC at $X_{Chol}$ of 5% or 60% was no greater than the difference found in the absence of Chol. At $X_{Chol} = 30\%$, where $L_\alpha^d$ and $L_\alpha^o$ coexist, $S_{CD}^{3-7}$ in SM was significantly higher than in DPPC. The higher $S_{CD}^{3-7}$ value in SM, as well as the higher-order parameters for the remainder of the chain, except for the two terminal carbons, could suggest either that SM per se was more ordered or that the pool size ratio of $L_\alpha^o/L_\alpha^d$ was larger compared to DPPC at this mixing ratio. Either possibility suggests a stronger interaction between SM and Chol at this mixing ratio range. Because high concentrations of Chol ($X_{Chol} \sim$ 30-50%) are found in the plasma membranes of most cell types, our data support the general hypothesis that Chol could interact more strongly with SM in biological membranes (Roper et al., 2000; Simons and Ikonen, 2000).

## H-Bonding between Chol and DPPC or SM

Many studies have attempted to determine whether there is direct H-bonding between the OH of Chol and the carboxyl in DPPC or the amide in SM, (e.g., Bhattacharya and Haldar, 2000; Dimitrov and Lalchev, 1998). On the basis of NMR studies, we proposed that direct H-bonding between Chol and DPPC was unlikely (Guo and Hamilton, 1995). This work shows that at $X_{Chol} < 22\%$, Chol had no effects on $\delta_{CO}$ (Fig 5 and 6), implying an absence of strong H-bonding between Chol and the amide group of SM. At $X_{Chol} > 22\%$, the $^{13}$C chemical shift of the amide group shifts downfield with $X_{Chol}$, similar to the result for the *sn*2 carbonyl of DPPC (Guo and Hamilton, 1996). Although this could be an indication of H-bonding with Chol, it could also be caused by other factors. For instance, in the absence of Chol, the electron-rich oxygen or nitrogen in SM can be H-bonded to the surrounding $H_2O$ molecules, which may also be H-bonded to each other. Insertion of Chol perturbs this water layer, and Chol-OH becomes H-bonded with surrounding $H_2O$ molecules. These effects could account, in part, for the changes in chemical shift of carbons in the interfacial region of the SM or DPPC molecules. The small difference in the quadrupolar splitting ($\Delta\nu_Q^{OD}$) of Chol-OD in SM and DPPC bilayers (Fig. 7 *D*) could reflect slightly different hydration states at the bilayer surface without the formation of specific H-bonds between Chol and SM. They do not suggest formation of a strong, specific H-bond with the amide. Others have found that the miscibility of Chol in SM is the same after the replacement of the amide with an ether linkage (Bittman et al., 1994). This indirectly suggests that H-bonding between Chol and the SM is not a significant determinant of interactions between the two lipids.

## Saturation limit of Chol in SM and the detection of crystalline Chol monohydrate

An important conclusion derived from the $^{13}$C-MASNMR results was that SM bilayers are not able to incorporate higher levels of Chol than DPPC bilayers in a noncrystalline form. As shown in Figs. 5 and 6, the chemical shifts of several carbons in both SM and Chol plateau at $X_{Chol} \sim$ 50%, suggesting that increasing Chol beyond $X_{Chol} = 50\%$

did not affect the SM-Chol interactions significantly. Distinctive C5 and C6 signals of Chol monohydrate (Fig. 4) were detected by CPMASNMR at $X_{Chol} = 60\%$ with signal intensities in proportion to increasing $X_{Chol}$. By extrapolation, crystallization began at $X_{Chol} \sim 50\%$. Therefore, the saturation limit of Chol in SM is the same as that in the bilayers of DPPC (Guo and Hamilton, 1995) and egg PC (Bourgès et al., 1967), consistent with the conclusions drawn from calorimetric (McIntosh et al., 1992; Oldfield and Chapman, 1971) and elastomechanical (Needham and Nunn, 1990) studies.

It is not clear where the Chol monohydrate crystals are localized in SM, as the excess Chol did not affect any of the measured NMR quantities. Because the longer and asymmetric hydrocarbon chains of SM create a 25% thicker core than DPPC and increased free volume in the center of the bilayer (Shipley et al., 1974; Schmidt et al., 1977), it is possible that small clusters of Chol crystals could localize in this region. Small aggregates of Chol crystals have been suggested to form laterally segregated domains in PC bilayers (Tulenko et al., 1998) or to be localized near the phosphate group in the aqueous interbilayer region (Guo and Hamilton, 1995). The later hypothesis was based on the marked broadening of the broadline spectrum of $^{31}$P-DPPC bilayers after Chol monohydrate crystals formed (Guo and Hamilton, 1995). Such a perturbation of the $^{31}$P-NMR resonance of SM was not observed.

## CONCLUSIONS

Phosphatidylcholine, sphingomyelin, and cholesterol are the major constituents of the plasma membrane in mammalian cells, serving as both structural matrix and signaling molecules. Recently, a number of laboratories have isolated membrane "rafts" as detergent-insoluble domains containing almost exclusively cholesterol-saturated sphingomyelin together with transmembrane or lipid-anchored proteins (Dobrowsky, 2000; Roper et al., 2000; Simons and Ikonen, 2000). While strongly implying a close interaction between Chol and SM (as opposed to other phospholipids), it is not clear to what extent the proteins mediate such interactions. In this study we compared the lipid-lipid interactions in the two model membranes of brain SM-Chol and DPPC-Chol. Most of our results highlight similarities rather than differences between these two systems. This does not rule out potential differences in other time frames or other chemical environments. In addition, our study compared a natural SM with synthetic DPPC to match the $T_m$ values in the two systems. PC molecules in biological membranes are rich in kinked unsaturated acyl chain whereas sphingomyelin contains mainly saturated acyl chains, a significant fraction of which are longer than 16 carbons. In such an environment, Chol will preferentially interact with sphingomyelin molecules to maximize the hydrophobic interactions.

This work was supported by National Institutes of Health Grant RO1 HL41904 (to J.A.H.) and RO1 DK45936 (to A.H.N.).

## REFERENCES

Ahmed, S. N., D. A. Brown, and E. London. 1997. On the origin of sphingolipid/cholesterol-rich detergent-insoluble cell membranes: physiological concentrations of cholesterol and sphingolipid induce formation of a detergent-insoluble, liquid-ordered phase in model membrane. *Biochemistry.* 36:10944–10953.

Aureli, T., M. Di Cocco, G. Capuani, R. Ricciolini, C. Manetti, A. Micheli, and F. Conti. 2000. Effect of long-term feeding with acetyl-L-carnitine on the age-related changes in rat brain lipid composition: a study by 31P NMR spectroscopy. *Neurochem. Res.* 25:395–399.

Bhattacharya, S., and S. Haldar. 2000. Interactions between cholesterol and lipids in bilayer membranes. Role of lipid headgroup and hydrocarbon chain-backbone linkage. *Biochim. Biophys. Acta.* 1467:39–53.

Bittman, R., C. R. Kasireddy, P. Mattjus, and J. P. Slotte. 1994. Interaction of cholesterol with sphingomyelin in monolayers and vesicles. *Biochemistry.* 33:11776–11781.

Böttcher, C. J. F., and C. M. van Gent. 1961. Changes in the composition of phospholipids and of phospholipid fatty acids associated with atherosclerosis in the human aortic wall. *J. Atheroscler. Res.* 1:36–46.

Bourgès, M., D. M. Small, and D. G. Dervichian. 1967. Biophysics of lipidic association. II. The ternary systems: cholesterol-lecithin-water. *Biochim. Biophys. Acta.* 137:157–167.

Calhoun, W. I. and G. G. Shipley. 1979. Sphingomyelin-lecithin bilayers and their interaction with cholesterol. *Biochemistry.* 18:1717–1722.

Chao, F. F., E. J. Blanchette, Y. J. Chen, B. F. Dickens, E. Berlin, L. M. Amende, S. I. Skarlatos, W. Gamble, J. H. Resau, and W. T. Mergner. 1990. Characterization of two unique cholesterol-rich lipid particles isolated from human atherosclerotic lesions. *Am. J. Pathol.* 136: 169–179.

Cullis, P. R., and M. J. Hope. 1980. The bilayer stabilizing role of sphingomyelin in the presence of cholesterol. *Biochem. Biophys. Acta.* 597:533–542.

Davis, J. H. 1991. Deuterium nuclear magnetic resonance spectroscopy in partially ordered systems. *In Isotopes in the Physical and Biomedical Sciences,* Vol. 2. E. Buncel and J. R. Jones, editors. Elsevier Science Publishers B.V., Amsterdam.

Dimitrov, O., and Z. Lalchev. 1998. Interaction of sex hormones and cholesterol with monolayers of dipalmitoylphosphatidylcholine in different phase states. *J. Steroid Biochem. Mol. Biol.* 66:55–61.

Dobrowsky, R. 2000. Sphingolipid signalling domains floating on rafts or buried in caves? *Cell Signal.* 12:81–90.

Dufourc, E. J., E. J. Parish, S. Chitrakorn, and I. Smith. 1984. Structural and dynamical detail of cholesterol-lipid interaction as revealed by deuterium NMR. *Biochemistry.* 23:6062–6071.

Forbes, J., J. Bower, X. Shan, L. Moran, E. Oldfield, and M. A. Moscarello. 1988. Some new developments in solid-state nuclear magnetic resonance spectroscopic studies of lipids and biological membranes, including the effects of cholesterol in model and natural systems. *J. Chem. Soc., Faraday Trans. I.* 84:3821–3849.

Griffin, R. G., L. Powers, and P. S. Pershan. 1978. Head-group conformation in phospholipids: a phosphorus-31 nuclear magnetic resonance study of oriented monodomain dipalmitoylphosphatidylcholine bilayers. *Biochemistry.* 17:2718–2722.

Guo, W., and J. A. Hamilton, 1995. A multinuclear solid-state NMR study of phospholipid-cholesterol interactions. Dipalmitoylphosphatidylcholine-cholesterol binary system. *Biochemistry.* 34:14174–14184.

Guo, W., and J. A. Hamilton. 1996. $^{13}$C MAS NMR studies of crystalline cholesterol and lipid mixtures modeling atherosclerotic plaques. *Biophys. J.* 71:2857–2868.

Huang, J., J. T. Buboltz, and G. W. Feigenson. 1999. Maximum solubility of cholesterol in phosphatidylcholine and phosphatidylethanolamine bilayers. *Biochim. Biophys. Acta.* 1417:89–100.

Huang, T.-H., C. Lee, S. K. Das Gupta, A. Blume, and R. G. Griffin. 1993. A $^{13}C$ and $^{2}H$ nuclear magnetic resonance study of phosphatidylcholine/cholesterol interactions: characterization of liquid-gel phases. *Biochemistry.* 32:13277–13287.

Hui, S. W. 1993. *Visualization of cholesterol domains in model membranes. In Cholesterol in Membrane Models. L. Finegold,* editor. CRC Press, Boca Reton. 159–172.

Keelan, M. and M. T. Clandinin. 1997. Refeeding varying fatty acid and cholesterol diets alters phospholipids in rat intestinal brush border membrane. *Lipids.* 32:895–901.

Kurze, V. 1998. *Untersuchungen zur Hydratation orientierter Phospholipidmembranen mittels magnetischer Kernresonanzspektroskopie.* Ph.D. thesis, Ludwig-Maximilians-Universität München.

Kurze, V., B. Steinbauer, T. Huber, and K. Beyer. 2000. A $^{2}H$ NMR study of macroscopically aligned bilayer membranes containing interfacial hydroxyl residues. *Biophys. J.* 78:2441–2451.

Lande, M. B., J. M. Donovan, and M. L. Zeidel. 1995. The relationship between membrane fluidity and permeabilities to water, solutes, ammonia, and protons. *J. Gen. Physiol.* 106:67–84.

Lange, Y., J. S. D'Alessandro, and D. M. Small. 1979. The affinity of cholesterol for phosphatidylcholine and sphingomyelin. *Biochim. Biophys. Acta.* 556:388–398.

Leppimäki, P., R. Kronqvist, and J. P. Slotte. 1998. The rate of sphingomyelin synthesis de novo is influenced by the level of cholesterol in cultured human skin fibroblasts. *Biochem. J.* 335:285–291.

Levi, M., D. M. Jameson, and B. W. van der Meer. 1989. Role of BBM lipid composition and fluidity in impaired renal Pi transport in aged rat. *Am. J. Physiol. Renal Physiol.* 256:F85–F89.

Lewin, M. and P. S. Timiras. 1984. Lipid changes with aging in cardiac mitochondrial membranes. *Mech. Ageing Dev.* 24:343–351.

Lund Katz, S., H. M. Laboda, L. R. McLean, and M. C. Phillips. 1988. Influence of molecular packing and phospholipid type on rates of cholesterol exchange. *Biochemistry.* 27:3416–3423.

Mantsch, H., H. Saito, and I. Smith. 1977. Deuterium magnetic resonance, applications in chemistry, physics and biology. *Progr. NMR Spectr.* 11:211–271.

Marsan, M. P., I. Muller, C. Ramos, F. Rodriguez, E. J. Dufourc, J. Czaplicki, and A. Milon. 1999. Cholesterol orientation and dynamics in dimyristoylphosphatidylcholine bilayers: a solid-state deuterium NMR analysis. *Biophys. J.* 76:351–359.

McIntosh, T. J., S. A. Simon, D. Needham, and C. H. Huang. 1992. Structure and cohesive properties of sphingomyelin/cholesterol bilayers. *Biochemistry.* 31:2012–2020.

Needham, D., and R. S. Nunn. 1990. Elastic deformation and failure of lipid bilayer membranes containing cholesterol. *Biophys. J.* 58: 997–1009.

Neuringer, L., B. Sears, F. Jungalwala, and E. Shriver. 1979. Difference in orientational order in phospholipid and sphingomyelin bilayers. *FEBS Lett.* 104:173–175.

Ohvo, H., and J. P. Slotte. 1996. Cyclodextrin-mediated removal of sterols from monolayers: effects of sterol structure and phospholipids on desorption rate. *Biochemistry.* 35:8018–8024.

Oldfield, E. and D. Chapman. 1971. Effects of cholesterol and cholesterol derivatives on hydrocarbon chain mobility in lipids. *Biochem. Biophys. Res. Commun.* 43:610–616.

Oldfield, E., M. Meadows, D. Rice, and R. Jacobs. 1978. Spectroscopic studies of specifically labeled membrane systems. Nuclear magnetic resonance investigation of the effects of cholesterol in model systems. *Biochemistry.* 17:2727–2740.

Prisco, D., P. G. Rogasi, M. Matucci, R. Paniccia, R. Abbate, G. F. Gensini, and G. G. Serneri. 1986. Age-related changes in platelet lipid composition. *Thromb. Res.* 44:427–437.

Roper, K., D. Corbeil, and W. Huttner. 2000. Retention of prominin in microvilli reveals distinct cholesterol-based lipid microdomains in the apical plasma membrane. *Nat. Cell Biol.* 2:582–592.

Sankaram, M. and T. E. Thompson. 1990. Interaction of cholesterol with various glycerophospholipids and sphingomyelin. *Biochemistry.* 29: 10670–10675.

Sankaram, M. B. and T. E. Thompson. 1991. Cholesterol-induced fluid phase immiscibility in membranes. *Proc. Natl. Acad. Sci. USA.* 88: 8686–8690.

Schmidt, C. F., Y. Barenholz, and T. E. Thompson. 1977. A nuclear magnetic resonance study of sphingomyelin in bilayer systems. *Biochemistry.* 16:2649–2656.

Schroeder, F. and G. Nemecz. 1989. Interaction of sphingomyelins and phosphatidylcholines with fluorescent dehydroergosterol. *Biochemistry.* 28:5992–6000.

Seelig, A. and J. Seelig. 1977. Effect of a single *cis* double bond on the structure of a phospholipid bilayer. *Biochemistry.* 16:45–50.

Shepherd, J. C. and G. Buldt. 1979. The influence of cholesterol on head group mobility in phospholipid membranes. *Biochim. Biophys. Acta.* 558:41–47.

Shipley, G. G., L. S. Avecilla, and D. M. Small. 1974. Phase behavior and structure of aqueous dispersions of sphingomyelin. *J. Lipid Res.* 15: 124–131.

Simons, K. and E. Ikonen. 2000. How cells handle cholesterol. *Science.* 290:1721–1726.

Slotte, J. P. 1992. Enzyme-catalyzed oxidation of cholesterol in mixed phospholipid monolayers reveals the stoichiometry at which free cholesterol clusters disappear. *Biochemistry.* 31:5472–5477.

Tulenko, T. N., M. Chen, P. E. Mason, and R. P. Mason. 1998. Physical effects of cholesterol on arterial smooth muscle membranes: evidence of immiscible cholesterol domains and alterations in bilayer width during atherogenesis. *J. Lipid Res.* 39:947–956.

VanderHart, D. L. 1981. Influence of molecular packing on solid-state $^{13}C$ chemical shifts: the *n*-alkanes. *J. Magn. Reson.* 44:117–125.

Vist, M. R. and J. H. Davis. 1990. Phase equilibria of cholesterol/dipalmitoylphosphatidylcholine mixtures: $^{2}H$ nuclear magnetic resonance and differential scanning calorimetry. *Biochemistry.* 29:451–464.

Wheeler, O. H. and J. L. Mateos. 1958. Stereochemistry of reduction of ketones by complex metal hydrides. *Can. J. Chem.* 36:1431–1435.